University of Baghdad
College of Engineering
JE
JOURNAL OF ENGINEERING

Journal of Engineering

journal homepage: www.jcoeng.edu.iq

Volume 32 Number 4 April 2026

Assessment of Inlet Baffle Configurations on Hydraulic Characteristics of a Rectangular Gravity Separator Using CFD

Muna S. Resin[1,*], **Haitham A. Hussein**[1], **Mohd Remy Rozainy Bin Mohd Arif Zainol**[2]

[1]Department of Civil Engineering, College of Engineering, Al-Nahrain University, Baghdad, Iraq
[2]School of Civil Engineering, Universiti Sains Malaysia, Nibong Tebal, Seberang Perai Selatan, Malaysia

ABSTRACT

Rectangular gravity separators are commonly used within wastewater treatment systems to remove fat, oil, and grease from water. The performance of these vessels is dependent to a great extent on the uniformity of the flow, since turbulence and recirculating eddies tend to break drops together, thus reducing the separation efficiency. Therefore, adding the inlet baffle is a feasible way to improve the hydraulic stability in the separator. To simulate the characteristics of flow in the gravity separator tanks, a two-dimensional computational fluid dynamics (CFD) model of a single-phase flow has been developed with Flow-3D (v11.04). The numerical model employed was based on the Finite Volume Method (FVM), used the Volume of Fluid (VOF) technique to simulate the free surface behavior, and implemented an RNG k–ε turbulence model. Flow behavior was analyzed using three parameters: the velocity standard deviation, which denotes the flow uniformity, the percentage of recirculation zones corresponding to mixing and stability, and kinetic energy distribution. The results showed that the baffle with two apertures provided the best hydraulic performance by minimizing velocity fluctuations and cross-flowing and also kinetic energy distribution. Thus, this arrangement was determined to be the most effective design in promoting the flow stability and separation performance inside a rectangular gravity separator.

Keywords: Computational fluid dynamics, Gravity separation tank, Inlet baffle, Oil–water separator, Perforated baffle.

1. INTRODUCTION

Oil and grease contamination is considered a major environmental problem occurring in drinking water facilities as well as in natural aquatic systems. The accumulation of these substances can lead to sewer blockages, reduced efficiency of treatment processes, and negative impacts on aquatic ecosystems **(Jameel et al., 2011; Keener et al., 2008; Mattsson et al., 2014; Mohana et al., 2023; Hartal et al., 2023; He et al., 2017; Yousefelahiyeh et al., 2017)**. Gravity separators are commonly used as one of the simplest and most widely applied treatment technologies to address these problems **(Metcalf and**

*Corresponding author
Peer review under the responsibility of University of Baghdad.
https://doi.org/10.31026/j.eng.2026.04.01

Article received: 31/01/2026
Article revised: 22/03/2026
Article accepted: 27/03/2026
Article published: 01/04/2026

Eddy, 2014). The distribution of flow within the separation chamber is an important factor affecting the hydraulic efficiency of separators. Excessive turbulence and the formation of recirculation zones reduce the effective hydraulic residence time, hinder droplet coalescence, and consequently reduce separation performance **(Wilkinson et al., 2000; Mee and Nor, 2011).**

Previous investigations have demonstrated that separator performance is highly sensitive to baffle configuration. Variations in baffle geometry can significantly influence separation efficiency **(Wilkinson et al., 2000)**. The use of perforated baffles has also been shown to suppress internal flow disturbances within the separator **(Mee and Nor, 2011)**. In addition, the relative position of baffles plays an important role in controlling the formation and intensity of recirculation zones inside the separator **(Hussein et al., 2013)**. More recent studies confirmed that, when properly designed, perforated baffles may outperform solid plates in improving separation performance **(Efendioglu et al., 2014; Al-Yacouby and Ahmed, 2022; Kim et al., 2025; Nascimento et al., 2025)**. However, these studies mainly focused on general baffle geometry, material characteristics, or overall porosity ratios rather than examining the specific hydraulic influence of the number of perforations .From a hydraulic perspective, the number of perforations in a baffle directly affects the fragmentation of the incoming jet, the dissipation of momentum, and the redistribution of velocity downstream of the plate. Changes in the number of openings may therefore alter turbulence intensity, the development of recirculation zones, and the overall uniformity of the flow field inside the separator. Despite this potential influence, the hydraulic implications of simplified perforated baffle configurations with limited numbers of openings have not been systematically investigated. This highlights the significance of baffles in separation equipment **(Solov'eva et al., 2021)**. However, relatively little attention has been given to simplified perforated baffle designs with reduced numbers of openings.

Therefore, the present study addresses this gap by examining the hydraulic performance of a rectangular gravity separator equipped with three inlet baffle configurations: a solid plate, a perforated plate with three openings, and a perforated plate with two openings. The simulations were performed using Computational Fluid Dynamics (CFD) with the Volume of Fluid (VOF) technique. Flow conditions were evaluated using two hydraulic indicators, namely the standard deviation of streamwise velocity and the recirculation zone ratio, which represent measures of flow uniformity and separation performance.

2. MATERIALS AND METHOD

2.1 Mathematical Model

2.1.1 Governing Equations

The Flow-3D model framework is based on mass continuity within the Reynolds-averaged Navier–Stokes (RANS) equations for incompressible viscous flows. Collectively, these governing equations conserve mass and momentum throughout the velocity field **(Selim et al., 2024; Zhang et al., 2023)**. The RANS method improves the traditional Navier–Stokes expression to take into consideration that the Reynolds stress has influence and thus is a much better representation of turbulent flow **(Hussein et al., 2015; Versteeg, 2007; Fang et al., 2020; Li et al., 2022; Mir Emad et al., 2025)**.

2.1.1.1 Mass Continuity Equation

The generalized continuity equation, leading to the mass conservation of fluid within the computational region, can be written **(Shahrokhi et al., 2012; Hirt and Nichols, 1981; Hirt and Sicilian, 1985; Wahba, 2022)** as follows:

$$V_f \frac{\partial \rho}{\partial t} + \frac{\partial}{\partial x}(\rho u A_x) + \frac{\partial}{\partial z}(\rho u A_z) = 0 \quad (1)$$

Here, ρ denotes the fluid density, u and w are the velocity components along the x- and z-directions, respectively, and Vf represents the fluid volume fraction within a computational cell.

2.1.1.2 Momentum Equations:

In a two-dimensional computational domain, the momentum equations, expressed in the form of the Navier–Stokes equations, can be written as **(Tsega, 2024)**:

$$\frac{\partial u}{\partial t} + \frac{1}{V_f}\{uA_x \frac{\partial u}{\partial x} + wA_Z \frac{\partial u}{\partial z} = -\frac{1}{\rho}\frac{\partial P}{\partial x} + G_x + f_x \quad (2)$$

$$\frac{\partial w}{\partial t} + \frac{1}{V_f}\left\{uA_x \frac{\partial w}{\partial x} + wA_Z \frac{\partial w}{\partial z}\right\} = -\frac{1}{\rho}\frac{\partial P}{\partial x} + G_z + f_z \quad (3)$$

Here, the viscous acceleration terms are given by f_x and fz, while the gravitational accelerations are denoted by Gx and Gz. The dynamic viscosity μ is defined by the formulas below:

$$\rho V_f f_x = wsx - \left\{\frac{\partial}{\partial x}(A_x \tau_{xx}) + \frac{\partial}{\partial z}(A_z \tau_{xz})\right\} \quad (4)$$

$$\rho V_f f_z = wsz - \left\{\frac{\partial}{\partial x}(A_z \tau_{xz}) + \frac{\partial}{\partial z}(A_z \tau_{zz})\right\} \quad (5)$$

where

$$\tau_{xx} = -2\mu \frac{\partial u}{\partial x}, \tau_{zz} = -2\mu \frac{\partial w}{\partial x}, \tau_{xz} = -\mu\{\frac{\partial u}{\partial z} + \frac{\partial w}{\partial x}\}$$

Where wsx and wsz represent the wall shear stress values applied in the x- and z-directions, respectively.

The air-water interface was dynamically modeled by means of the VOF method, which could precisely capture the movement of the interface through time during the numerical simulation. In this way, the accurate depiction of the free-surface profile in the computational domain is achieved. As for what concerns the VOF equation, it represents an evolution equation of the volume fraction field **(Azimi and Shabanlou, 2020; Fluent, 2009; Torres et al., 2021; Roy-Biswas and Singh, 2025)**.

$$\frac{\partial F}{\partial t} + \frac{1}{V_f}\left\{\frac{\partial}{\partial x}(FA_x u) + \frac{\partial}{\partial z}(FA_z w)\right\} = 0 \quad (6)$$

The tank internal geometry, with solid or perforated baffles, was described using the Fractional Area/Volume Obstacle Representation (FAVOR) method. In this approach, solid boundaries are integrated in the structured mesh by means of fractional cell volumes and face areas to give an accurate representation of fluid–solid interfaces present within the simulation domain **(Hirt and Sicilian, 1985; Nimisha et al., 2022)**.

2.1.2 Turbulence Model

The RNG (Reynold's stress) k–ε model was used as the modified form of the standard k–ε model in this work. It is frequently used to predict the turbulent hydraulic flows with recirculation due to its stability and enhanced predictive capability when compared with the conventional model **(Laleh et al., 2012)**. The model describes turbulence by two transport equations: one for the turbulent kinetic energy (k), which is an indication of the amount of velocity fluctuations, and the other for the dissipation rate (ε), which represents the pace at which turbulent energy is wasted **(Hussein et al., 2013**). A significant related advantage of the RNG method is that it has marginal reliance upon empirically determined constants, leading to a more systematic statistical foundation and increasing the reliability of simulations for high Reynolds number flows **(Yakhot and Orszag, 1986; Yakhot et al., 1992)**. The RNG k–ε model equations are given by Eqs. (7) and (8):

$$\frac{\partial k}{\partial t} + \frac{1}{Vf} + \left\{uAx\frac{\partial k}{\partial x} + uAz\frac{\partial k}{\partial z}\right\} = p + Diff - \mathcal{E} \tag{7}$$

$$\frac{\partial \mathcal{E}}{\partial t} + \frac{1}{Vf}\left\{uAx\frac{\partial\, \mathcal{E}}{\partial x} + uAz\frac{\partial \mathcal{E}}{\partial z}\right\} = \mathrm{C}_{1\mathcal{E}}\frac{p\mathcal{E}}{k} + DDif - C_{2\mathcal{E}}\frac{\mathcal{E}^2}{k} \tag{8}$$

The most significant parameters considered in this study are the dissipation rate (ε), turbulent kinetic energy (k), gravitational acceleration (G), and pressure (P). The RNG model includes model constants defined as $C1\varepsilon$=1.42, $C2\varepsilon$=1.68, and $C3\varepsilon$=0.2 **(Yakhot and Orszag, 1986)**.

2.2 Numerical Model

The progressive improvement of numerical procedures has led to CFD becoming a well-established and widely accepted tool in the industrial community. Conventional flow measurements require complex and expensive instrumentation, whereas CFD methods afford a more versatile and less expensive one. It is also more generally applicable than the semi-empirical models employed in many separator designs **(Acharya and Casimiro, 2020)**. The physical space of the separation tank in this study was transformed into an equivalent discretized computational mesh, and the governing equations were solved using FLOW-3D (version 11.04). The flow field was described by the incompressible Navier–Stokes equations. The RANS-based method was used to model turbulence using the RNG k–ε closure **(Hussein et al., 2013; Yakhot and Orszag, 1986)**. The free surface was modeled using the VOF method **(Hirt and Nichols, 1981)**, and solid structures like baffles and inlets were represented according to FAVOR (Fractional Area/Volume Obstacle Representation) for an accurate geometry representation. These numerical schemes together formed a complete system and served as fertile ground for the examination of velocity distribution, fluid motion characteristics, and separation efficiency.

2.2.1 Computational Model

The separation tank was modeled as a three-dimensional rectangular-shaped region with a length of 2.0 m, a depth of 0.5 m, and a width of 0.5 m. **Fig. 1** shows the geometry of the separation tank. The inflow boundary was located along the left vertical wall, where a uniform horizontal velocity with a value of 0.04 m/s corresponding to a discharge rate of Q = 0.002 m^3/s has been imposed, and the outlet was represented on the right side (bottom), placed at 0.45 m from the bottom to allow surface water withdrawal. Another vertical baffle

was installed near the outlet in order to keep a constant hydraulic condition, and it rose 0.1 m above the bottom of the tank.

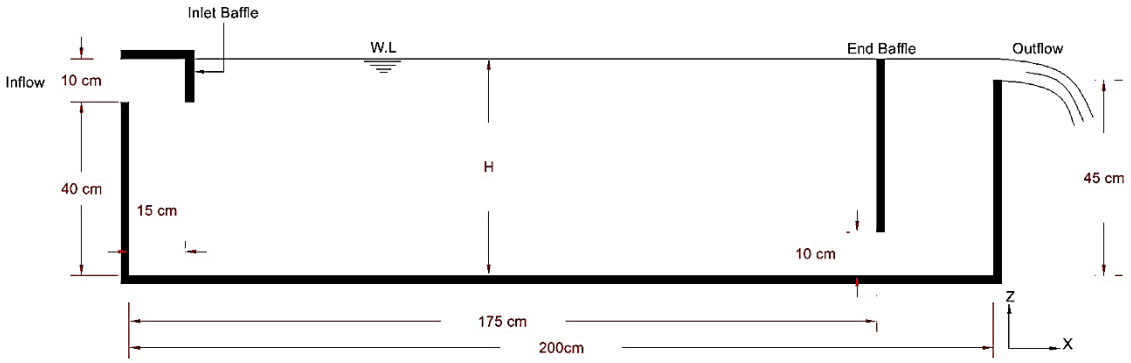

Figure 1. Longitudinal section of gravity separation tank.

The geometry of the tank was modeled using the FLOW-3D platform, as explained in Appendix A, which shows the complete CFD setup in the FLOW-3D platform. The perforated baffles were designed using AutoCAD in three dimensions and then exported in STL format, which is the only format that the FLOW-3D platform can be investigated in the present research, as shown in **Fig. 2**. In the former arrangement, a solid vertical baffle was installed at 0.15 m downstream of the corner as shown in **Fig. 2a**. For the second case, the baffle had three equally sized circular perforations, as shown in **Fig. 2b**, and a similar configuration was adopted for the third one with two circular openings, as shown in **Fig. 2c**. In both the perforated cases, the hole diameter of two-dimensional openings was kept constant at 0.06 m. For all setups, the height of baffles above the tank bottom was set at 0.4 m to have identical hydraulic conditions and a common base for comparison in the study.

These three configurations were chosen to create a consistent comparison of the variation between solid and perforated baffles with different hole quantities. This was with the aim of evaluating their effects on the velocity field inside the tank and the overall separation efficiency of the rectangular gravity separator.

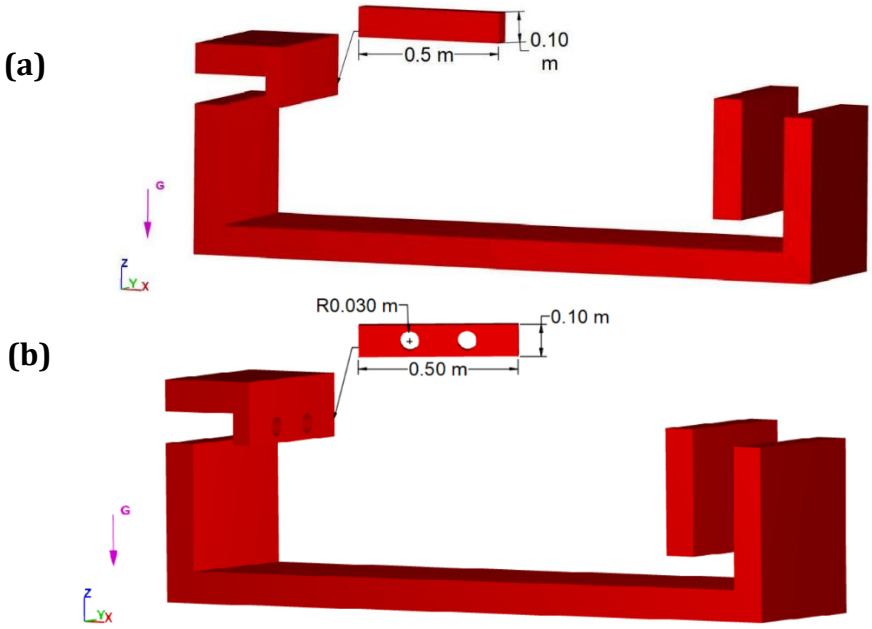

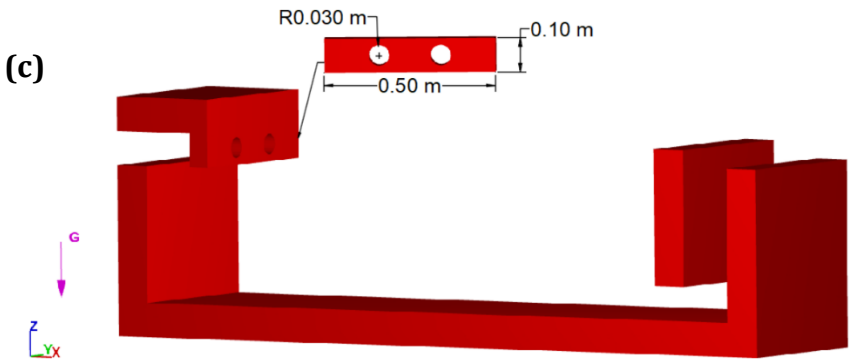

Figure 2. Separation tank geometry with different inlet baffle configurations (a) solid baffle, (b) perforated baffle with 3 holes, and (c) perforated baffle with 2 holes

The reliability of the developed numerical model was confirmed by comparing the simulated velocity distributions, obtained using the RNG k–ε turbulence closure, with the experimental measurements **(Shahrokhi et al., 2012)**.

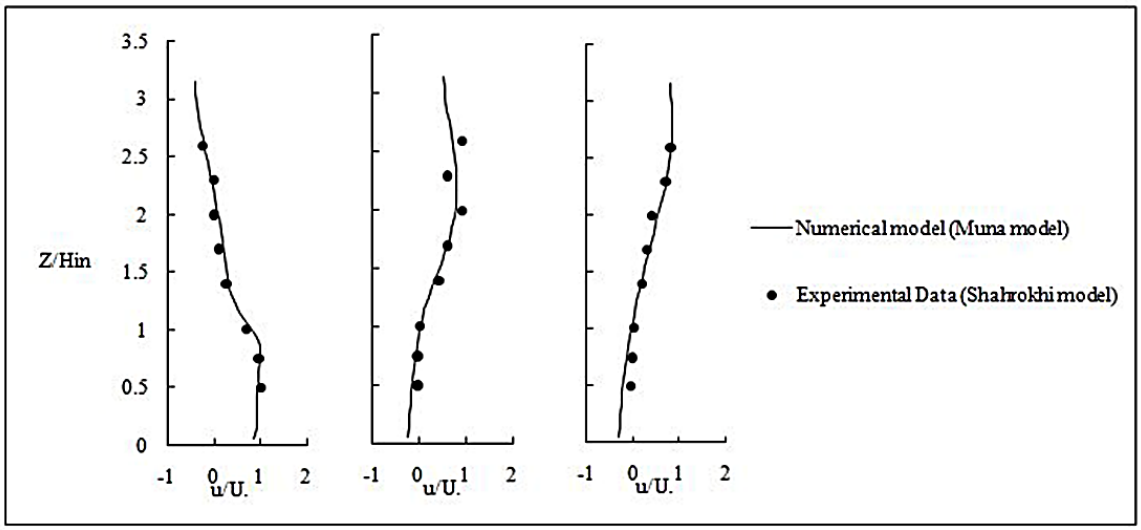

Figure 3. Validation of simulated and experimental velocity measurements.

Fig. 3 shows a clear agreement between the numerical predictions and the experimental data, where both the correlation coefficient and the coefficient of determination (R = 0.98 and R^2 = 0.96) indicate high model accuracy, thereby reinforcing confidence in the adopted computational approach and justifying its application in the present study.

2.2.2 Mesh Generation

The computational domain was discretized in a structured mesh of rectangular elements, as shown in **Fig. 4a**. Base cell dimensions of 0.03 m were used in both directions, which resulted in a total of 9,625 cells over the whole computational domain. Adjoint solutions to increase resolution, the mesh was homogenized around the inlet baffle, as shown in **Fig. 4b** at cell size 0.02 m, generating approximately 1150 cells in that region. An additional course with a spacing of 0.015 m was imposed near the perforation openings, which resulted in

approximately 490 cells to characterize properly all the velocity gradients and shear layers adjacent to the hole edges, as shown in **Fig. 4c**.

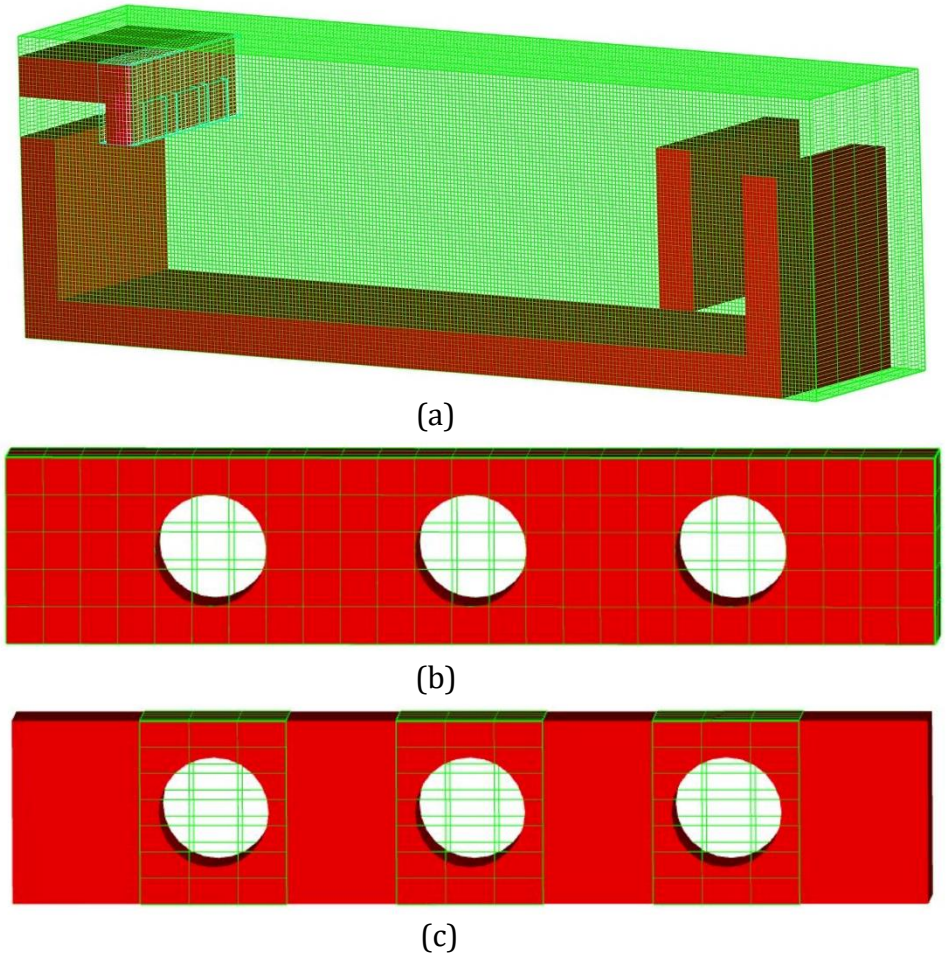

Figure 4. Numerical grid of the separation tank and inlet baffles for different perforations.

This model solidification refinement approach enabled the simulation to capture flow structures in regions of interest with better accuracy and maintain a reasonable overall computation time. The solid boundaries, such as the inlet baffles, were treated using the FAVOR method, which provides an exact geometry description within the mesh, as shown in **Fig. 5**.

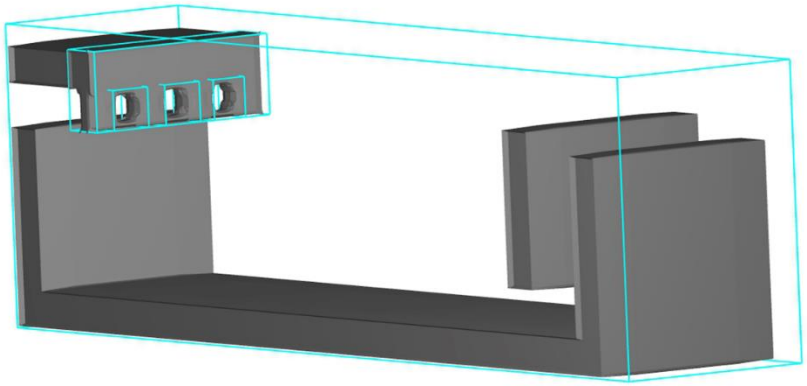

Figure 5. Separation tank computational domain described with the FAVOR tool.

2.2.3 Boundary Conditions

The boundary conditions used in numerical modeling are shown in **Fig. 6**. These were determined in this way to simulate the real hydraulic behavior of the separation tank, as produced under steady inflow conditions. The left boundary was given a uniform horizontal velocity of 0.04 m/s at the inlet. The outlet was placed on the right boundary and defined as an outflow boundary for surface water. The top wall was considered a free surface by the VOF model for tracking the interface motion. The bottom, sidewall, and baffle surfaces were set with no-slip conditions to mimic the solid boundary as non-penetration.

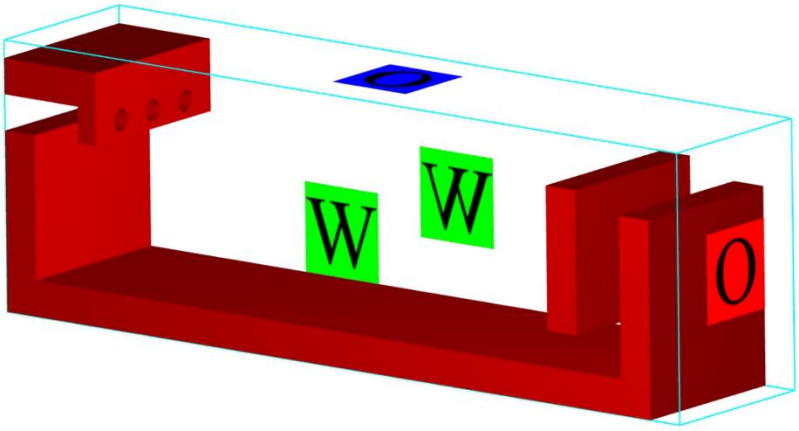

Figure 6. Conditions at the boundary of the Computational Domain for the separation tank.

3. RESULTS AND DISCUSSION

3.1 Velocity Profile Distribution

Stability of the horizontal velocity plays an important role in promoting droplet coalescence and separation efficiency, as it affects the growth and rise of oil droplets to a large extent **(Wilkinson et al., 2000; Ma et al., 2024; Xu et al., 2023)**.

Table 1. Velocity deviations in separation tank

Case	Description of inlet baffle	SD of x-velocity (m/s) ∗ E-02			
		Sections x(m)			
		0.2	0.6	1.2	1.6
a	Solid baffle	0.80	0.64	0.98	0.28
b	3 openings with a diameter of 6 cm	5.22	8.06	8.43	4.06
c	2 openings with a diameter of 6 cm	1.55	0.49	0.25	0.41

Table 1 presents the standard deviation for streamwise velocity with respect to three inlet baffle configurations. The standard deviation (σ) of the velocity along the flow direction (m/s) is calculated using the following formula:

$$\sigma = \sqrt{\frac{1}{N}\sum_{i=1}^{N}(U_i - \bar{U})^2} \quad (9)$$

where $U_i$is the velocity measured at the i^{th}point, $\bar{U}$is the mean velocity across all measurement points, $N$is the total number of measurement points along the flow direction. The findings indicated that the three-hole perforated baffle produced the greatest deviations

in the separation zone, indicating a very non-uniform flow distribution, which would lead to instability of the tank. This phenomenon is due to the formation of more complex flow patterns, as multiple small jets enter the tank simultaneously through the baffle openings. These jets interact to create regions of acceleration and deceleration, generating eddies and recirculation zones and consequently making the velocity field highly non-uniform with significantly higher standard deviation values. In contrast, the solid baffle recorded higher standard deviation values at the peripheral measurement sites, while the double-hole perforated baffle recorded the lowest differences (fluctuations) at the intermediate measurement sites, demonstrating continuity in flow homogeneity. which means dynamical patterns of velocity fields and hydraulic conditions were better, and consequently, the separation efficiency is improved. These results validate the use of standard deviation as an indicator for flow uniformity in separation tanks

3.2 Flow Field

The analysis of recirculation patterns provides further evidence of the effect of an inlet baffle design on the internal hydraulics of the separator. Recirculation zones are undesirable because they reduce the effective residence time and intensify internal mixing, thereby limiting separation efficiency **(Mee and Nor, 2011; Zhu et al., 2022)**. The streamline shown in **Fig. 7**, combined with the values in **Table 2**, illustrates clear differences among the three configurations.

Table 2. Recirculation zone percentages as influenced by inlet baffle configuration.

Cases	a) Sold baffle	b) Baffle with 3 openings	c) Baffle with 2 openings
Recirculation zone %	58	59	45

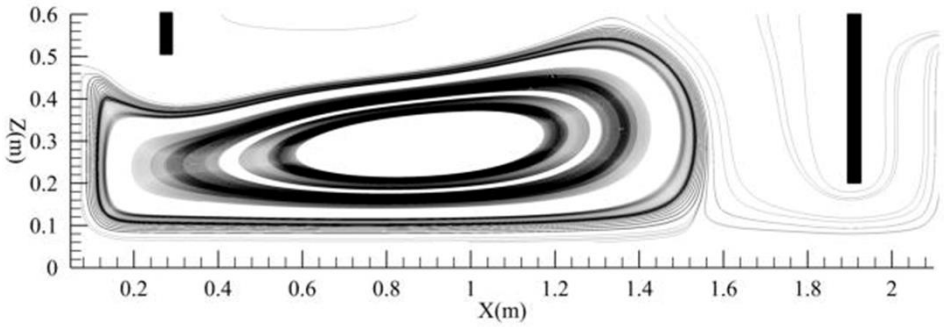

(a)

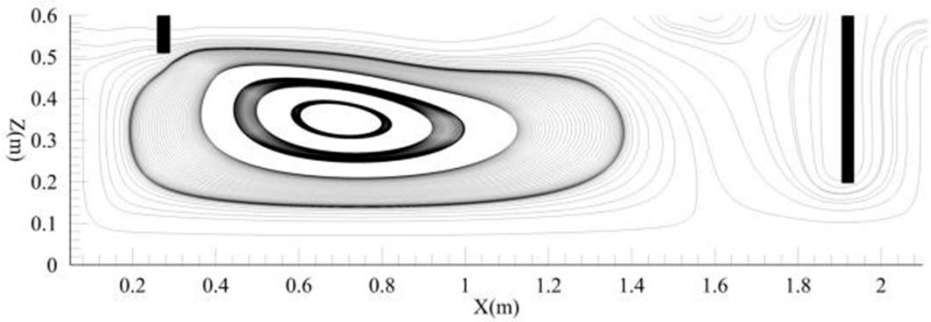

(b)

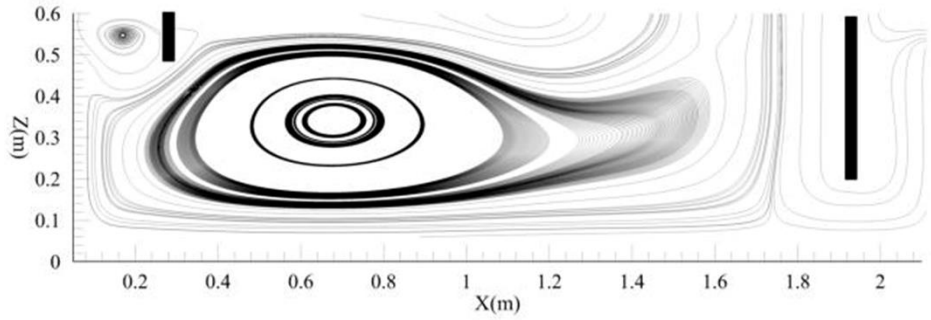

(c)

Figure 7. Flow streamlines for different inlet baffle configurations: (a) solid baffle, (b) perforated baffle with three holes, and (c) perforated baffle with two holes.

In the case of the two-hole perforated baffle as shown in **Fig. 7c**, the flow field was dominated by two circulation cells: a small surface vortex upstream of the plate and a more compact primary recirculation cell extending downstream. This configuration reduced the net circulation area by decreasing mesh openings, which did not exist in other schemes, and created a regular pattern for vortex shedding, resulting in its minimum percentage value compared to other structures given in **Table 2**. Meanwhile, the 3-hole baffle, as shown in **Fig. 7 b**, achieved the biggest recirculation zone that penetrated to the center of the tank and further promoted intensive internal circulation. The solid baffle, as shown in **Fig. 7a**, behaved as an intermediate case, featuring a high and quite stable vortex that retained part of the separation region. These findings underline that less recirculation leads to more homogeneous flow velocity and improved separation conditions and confirm the gain in hydraulic efficiency with a two-hole arrangement **(Efendioglu et al., 2014; Al-Yacouby and Ahmed, 2022; Chen et al., 2024)**.

3.3 Kinetic Energy

The kinetic energy represents an important factor for the separation tank under examination in this study. The three tested inlet baffle configurations were used with the aim of reducing kinetic energy within the tank, thus slowing down the flow while ensuring an equal fluid status **(Wilkinson et al., 2000)**.

Table 3. Kinetic Energy distribution along the separation tank

Case	Description of inlet baffle	KE (m^2/s^2) ∗ E-03			
		Sections x (m)			
		0.2	0.6	1.2	1.6
a	Solid baffle	74.80	78.90	64.40	0.05
b	3 openings with a diameter of 6 cm	1.43	2.91	3.38	7.77
c	2 openings with a diameter of 6 cm	0.18	0.09	0.02	0.14

Table 3. presents the values of kinetic energy (m^2/s^2) at specific points in the separation tank for the various baffle-hole arrangements. The use of a solid baffle will result in relatively higher kinetic energies, which will fall off gradually, indicating higher velocities in the incoming stream of fluid. The kinetic energies will fluctuate in value as the baffle has three holes, indicating a fall in value along the length of the separation tank. The use of the two-hole baffle will result in lower kinetic energies, indicating a higher fall in the value of the fluid velocity, which will result in a calm fluid with higher droplet cohesion.

4. CONCLUSIONS

The hydraulic performance of a rectangular oil-water separation unit was investigated with three types of inlet baffles: a solid baffle, the perforated baffle with three holes, and the perforated baffle with two holes. The aforesaid features were evaluated based on three leading parameters, namely, streamwise velocity standard deviation, recirculation zone ratio, and kinetic energy, which are the direct gauges of flow stability and separation efficiency, respectively. The results of the study showed that the three-hole baffle was the worst hydraulic condition, with each having significantly high velocity fluctuations, large circulation regions, and fluctuating kinetic energy. The solid baffle had a predictably intermediate efficiency to help reduce velocity variations in the local zones and, at the same time, provide an extended, stable vortex within the separation zone and increase kinetic energy. On the other hand, two-hole baffles provided optimal conditions, as they associated a smaller velocity fluctuation with a circulation area far more strictly limited, as well as kinetic energy. Finally, based on the performance analysis of these three baffle designs, it can be concluded that the design with two openings has a better performance by obtaining a more balanced distribution of the flow magnitude compared to the others and also generating favorable hydraulic conditions for easier de-oiling.

NOMENCLATURE

Symbol	Description	Symbol	Description
Vf	Volume of a fraction	τ_{xx}, τ_{xz}	Normal stress (x, z-direction) (N/m^2)
ρ	Fluid density (kg/m^3)	μ	Dynamics viscosity (Pa·s)
t	Time (s)	F	Volume fraction function (VOF)
x, z	Horizontal and Vertical coordinate (m)	k	Turbulent kinetic energy (m^2/s^2)
u, w	Velocity in x, z-direction (m/s)	$Diff$	Diffusion term of k (m^2/s^3)
A_x, A_z	Area in x, z-direction (m^2)	ε	Dissipation rate of turbulent kinetic energy (m^2/s^3)
P	Pressure (Pa)	$C1\varepsilon, C2\varepsilon, C3\varepsilon$	Empirical constant
p	Production of turbulent kinetic energy (m^2/s^3)	Q	discharge rate (m^3/s)
G_x, G_z	Body accelerations (m/s^2)	U	mean velocity (m/s)
fx, fz	Viscous acceleration (m/s^2)	SD	standard deviation (m/s)
wsx, wsz	Momentum source term (x, z-direction) (N/m^3)	KE	kinetic energy (m^2/s^2)

Acknowledgements

The authors would like to acknowledge the support provided by the Department of Civil Engineering, College of Engineering, Al-Nahrain University, Baghdad, Iraq, during the completion of this research

Credit Authorship Contribution Statement

Muna S. Resin: Conceptualization, Methodology, Numerical modeling, Software, Data analysis, writing original draft, Writing review & editing. Haitham A. Hussein: Methodology, Writing review & editing, Supervision. Mohd Remy Rozainy Bin Mohd Arif Zainol: Writing review & editing, Validation.

Declaration of Competing Interest

The authors declare that they have no known competing financial interests or personal relationships that could have appeared to influence the work reported in this paper.

REFERENCES

Acharya, T., Casimiro, L., 2020. Evaluation of flow characteristics in an onshore horizontal separator using computational fluid dynamics. *Journal of Ocean Engineering and Science*, 5, pp. 261-268. https://doi.org/10.1016/j.joes.

AL-Yacouby, A. M., Ahmed, M. M., 2022. A numerical study on the effects of perforated and imperforate baffles on the sloshing pressure of a rectangular tank. *Journal of Marine Science and Engineering*, 10, P. 1335. https://doi.org/10.3390/jmse10101335.

Azimi, H., Shabanlou, S., 2020. U-shaped channels along the side weir for subcritical and supercritical flow regimes. *ISH Journal of Hydraulic Engineering*, 26, pp. 365-375. https://doi.org/10.1080/09715010.2018.1493706.

Chen, S. Y., Shimizu, S., Watanabe, H., 2024. Adjoint-based topology optimization for hydraulic performance improvement in double-suction volute pump. In: *Fluids Engineering Division Summer Meeting*, American Society of Mechanical Engineers, V001T01A013. https://doi.org/10.1115/FEDSM2024-130597.

Efendioglu, A., Mendez, J., Turkoglu, H., 2014. The numerical analysis of the flow and separation efficiency of a two-phase horizontal oil-gas separator with an inlet diverter and perforated plates. *Advances in Fluid Mechanics*, 10, P. 133. https://doi.org/10.2495/AFM140121.

Fang, R., Sondak, D., Protopapas, P., Succi, S., 2020. Neural network models for the anisotropic Reynolds stress tensor in turbulent channel flow. *Journal of Turbulence*, 21, pp. 525-543. https://doi.org/10.1080/14685248.2019.1706742.

Fluent Ink., 2009. ANSYS Fluent 12.0 theory guide. Canonsburg, PA: ANSYS Inc.

Hartal, O., Souabi, S., Chatoui, M., Ettaloui, Z., Madinzi, A., Rifi, S. K., Kurniawan, T. A., Anouzla, A., 2023. Contamination reduction of vegetable oil refinery wastewater using innovative acid and basic chemical flotation processes. *Preprint.* https://doi.org/10.21203/rs.3.rs-3146896/v1.

He, X., De Los Reyes III, F. L., Ducoste, J. J., 2017. A critical review of fat, oil, and grease (FOG) in sewer collection systems: Challenges and control. *Critical Reviews in Environmental Science and Technology*, 47, pp. 1191-1217.

Hirt, C., Sicilian, J., 1985. A porosity technique for the definition of obstacles in rectangular cell meshes. In: Proceedings of the 4th International Conference on Numerical Ship Hydrodynamics.

Hirt, C. W., Nichols, B. D., 1981. Volume of fluid (VOF) method for the dynamics of free boundaries. *Journal of Computational Physics*, 39, pp. 201-225. https://doi.org/10.1016/0021-9991(81)90145-5.

Hussein, H. A., Abdullah, R., Harun, S., Abdulkhaleq, M., 2013. Numerical model of baffle location effect on flow pattern in oil and water gravity separator tanks. *World Applied Sciences Journal*, 26, pp. 1351-1356 . https://doi.org/10.5829/idosi.wasj.2013.26.10.1239.

Hussein, H. A., Abdullah, R., Md Said, M. A., 2015. Computational investigation of inlet baffle height on the flow in a rectangular oil/water separator tanks. *Applied Mechanics and Materials*, 802, pp. 587–592. https://doi.org/10.4028/www.scientific.net/AMM.802.587.

Jameel, A. T., Muyubi ,S. A., Karim, M. I. A., Alam, M. Z., 2011. Removal of oil and grease as emerging pollutants of concern (EPC) in wastewater stream. *IIUM Engineering journal*, 1. https://doi.org/10.31436/iiumej.v12i4.218.

Keener, K. M., Ducoste, J. J., Holt, L. M., 2008. Properties influencing fat, oil, and grease deposit formation. *Water environment research*, 80, pp. 2241-2246. https://doi.org/10.2175/193864708X267441.

Kim, S., Kim, H., Jeong, H. S., Kim, Y., 2025. Optimal design of perforated baffles for enhancing oil-water separation performance using genetic algorithms. *Results in Engineering*, 26, p. 10466. https://doi.org/10.1016/j.rineng.2025.104668.

Laleh, A. P., Svrcek, W. Y., Monnery, W. D., 2012. Design and CFD studies of multiphase separators—a review. *The Canadian Journal of Chemical Engineering*, 90, pp. 1547-1561.

Li, J.-P., Tang, D.-G., Yi, C., Yan, C., 2022. Data-augmented turbulence modeling by reconstructing Reynolds stress discrepancies for adverse-pressure-gradient flows. *Physics of Fluids*, 34.

Ma, H., Ma, Z., Zhao, Q., Li, Y., Zhu, K., Zhang, H., Chen, X., 2024. Arrow-shaped patterned microchannel for enhancing droplet coalescence and demulsification of oil-in-water emulsions with high oil content. *Colloids and Surfaces A*: *Physicochemical and Engineering Aspects*, 685, P. 133177. https://doi.org/10.1016/j.colsurfa.2024.133177.

Mattsson, J., Hedström, A., Viklander, M., Blecken, G.-T., 2014. Fat, oil, and grease accumulation in sewer systems :comprehensive survey of experiences of Scandinavian municipalities. *Journal of environmental engineering*, 140, P. 04014003. http://dx.doi.org/10.1061/(ASCE) EE.1943-7870.0000813.

Mee, C. G., Nor, M. I. M., 2011. Flow pattern in a horizontal primary separator with a perforated baffle. *Journal of the Institution of Engineers, Malaysia*, 72.

Metcalf, Eddy, A., 2014. Wastewater Engineering Treatment and Resource Recovery. New York: McGraw-Hill Education.

Mir Emad, M., Mazaheri, K., Darbandi, M., 2025. Assessment of algebraic anisotropic turbulent heat flux models using Reynolds stress modeling for simulating film cooling flows. *Physics of Fluids*, 37. https://doi.org/10.1063/5.0245045.

Mohana, A. A., Roddick, F., Maniam, S., Gao, L., Pramanik, B. K., 2023. Component analysis of fat, oil and grease in wastewater: challenges and opportunities. *Analytical Methods*, 15, pp. 5112-5128. https://doi.org/10.1039/D3AY01222K.

Nascimento ,J. B. D. S., Ferreira, A. D., Vasconcelos, A. L., De Farias Neto, S. R., 2025. Study of the influence of Semi-porous baffles on the three-phase separation efficiency in a horizontal separator vessel via CFD. *Journal of Petroleum Science and Technology* , 14(3), P. 50.

Nimisha, P., Jayalekshmi, B., Venkataramana, K., 2022. Slosh damping in rectangular liquid tank with additional blockage effects under pitch excitation. *Journal of Fluids Engineering,* 144, P. 121403. https://doi.org/10.1115/1.4054959.

Roy-Biswas, T., Singh, P., 2025. Volume of fluid approach for modeling nappe flow over hydraulic structures. *Physics of Fluids*, 37.

Selim, T., Hamed, A. K., Elkiki, M., Eltarabily, M. G., 2024. Numerical investigation of flow characteristics and energy dissipation over piano key and trapezoidal labyrinth weirs under free-flow conditions. *Modeling Earth Systems and Environment*, 10, pp. 1253-1272. https://doi.org/10.1007/s40808-023-01844-w.

Solov'eva, O. V., Solov'ev, S. A., Yafizov, R. R., Ponikarov, S. I. and Portnov, I. Y., 2021. Influence of design of baffles in a gravity-dynamic separator model on water-oil emulsion separation efficiency. *Chemical and Petroleum Engineering*, 56, pp. 884–888. https://doi.org/10.1007/s10556-021-00912-1

Shahrokhi, M., Rostami, F., Said, M. A. M., Yazdi, S. R. S., 2012. The effect of number of baffles on the improvement efficiency of primary sedimentation tanks. Applied Mathematical Modelling, 36, pp. 3725-3735. https://doi.org/10.1016/j.apm.2011.11.001.

Torres, C., Borman, D., Sleigh, A., Neeve, D., 2021. Application of three-dimensional CFD VOF to characterize free-surface flow over trapezoidal labyrinth weir and spillway. *Journal of Hydraulic Engineering*, 147, P. 04021002. https://doi.org/10.1061/(ASCE)HY.1943-7900.0001852.

Tsega, E. G., 2024. Advancing Finite Difference Solutions for Two-Dimensional Incompressible Navier–Stokes Equations Using Artificial Compressibility Method and Sparse Matrix Computation. *Journal of Applied Mathematics*, 2024(1), P. 5506715. https://doi.org/10.1155/2024/5506715.

Versteeg, H. K., 2007. An introduction to computational fluid dynamics the finite volume method, 2/E, Pearson Education India.

Wahba, E., 2022. Derivation of the differential continuity equation in an introductory engineering fluid mechanics course. *International Journal of Mechanical Engineering Education*, 50, pp. 538-547. https://doi.org/10.1177/03064190211014460.

Wilkinson, D., Waldie, B., Nor, M. M., Lee, H. Y., 2000. Baffle plate configurations to enhance separation in horizontal primary separators. *Chemical Engineering Journal*, 77, pp. 221-226.

Xu, H., Zhou, Y., Daniel ,D., Herzog, J., Wang, X., Sick, V., Adera, S., 2023. Droplet attraction and coalescence mechanism on textured oil-impregnated surfaces. *Nature Communications*, 14, P. 4901. https://pubs.acs.org/doi/10.1021/acsnano.3c07407.

Yakhot, V., Orszag, S. A., 1986. Renormalization group analysis of turbulence. I. Basic theory. *Journal of scientific computing*, 1(1), pp. 3-51. https://doi.org/10.1007/BF01061452.

Yakhot, V., Orszag, S. A., Thangam, S., Gatski, T., Speziale, C., 1992. Development of turbulence models for shear flows by a double expansion technique. *Physics of Fluids A: Fluid Dynamics*, 4, pp. 1510-152 0. https://doi.org/10.1063/1.858424.

Yousefelahiyeh, R., Dominic, C. C. S., Ducoste, J., 2017. Modeling fats, oil and grease deposit formation and accumulation in sewer collection systems. *Journal of Hydroinformatics*, 19, pp. 443-455.

Zhang, Y., Zhang, D., Jiang, H., 2023. Review of Challenges and Opportunities in Turbulence Modeling: A Comparative Analysis of Data-Driven Machine Learning Approaches. *Journal of Marine Science and Engineering*, 11. https://doi.org/10.3390/su151813384.

Zhu, D., Han, D., He, W., Chen, J., Ji, Y., Tao, P., Gu, Y., 2022. Performance analysis of the separator with inner channels by experiment and CFD-POST. *Energy Sources, Part A: Recovery, Utilization, and Environmental Effects*, 44, pp. 8527-8541. https://doi.org/10.1080/15567036.2022.2118908.

تقييم تكوينات الحواجز المدخلية على الخصائص الهيدروليكية لفاصل الجاذبية المستطيل باستخدام ديناميكا الموائع الحسابية

منى رسن[1,*]، هيثم حسين[1]، مهد ريني رزيني مهد عارف زينل[2]

[1]قسم الهندسة المدنية، كلية الهندسة، جامعة النهرين، بغداد، العراق

[2] مدرسة الهندسة المدنية، جامعة العلوم الماليزية، نيبونغ تيبال، سيبرنغ براي سيلاتان، ماليزيا

الخلاصة

تُستخدم فواصل الجاذبية المستطيلة بشكل شائع في أنظمة معالجة مياه الصرف الصحي لإزالة الزيوت والشحوم من الماء. يعتمد أداء هذه الأوعية إلى حد كبير على انتظام التدفق، حيث تميل الاضطرابات والدوامات الدائرية إلى تفتيت القطرات معًا، مما يقلل من كفاءة الفصل. لذلك، يُعدّ إضافة حاجز مدخل طريقة فعّالة لتحسين الاستقرار الهيدروليكي في الفاصل. لمحاكاة خصائص التدفق في خزانات فواصل الجاذبية، تم تطوير نموذج ثنائي الأبعاد لديناميكيات الموائع الحسابية (CFD) لتدفق أحادي الطور باستخدام برنامج Flow-3D (الإصدار 11.04). اعتمد النموذج العددي المستخدم على طريقة الحجم المحدود (FVM)، واستخدم تقنية حجم السائل (VOF) لمحاكاة سلوك السطح الحر، وطبّق نموذج اضطراب RNG k–ε. تم تحليل سلوك التدفق باستخدام ثلاثة معايير: الانحراف المعياري للسرعة الذي يدل على انتظام التدفق، ونسبة مناطق إعادة التدوير التي تُعنى بالخلط والاستقرار، وتوزيع الطاقة الحركية. أظهرت النتائج أن الحاجز ذو الفتحتين يوفر أفضل أداء هيدروليكي من خلال تقليل تقلبات السرعة والتدفق العرضي، بالإضافة إلى تقليل توزيع الطاقة الحركية. وبناءً على ذلك، تم تحديد هذا التصميم باعتباره الأكثر فعالية في تعزيز استقرار التدفق وأداء الفصل داخل فاصل الجاذبية المستطيل.

الكلمات المفتاحية: ديناميكا الموائع الحسابية, خزان الفصل بالجاذبية, حاجز المدخل, فاصل الزيت والماء, الحاجز المثقب.